

Journal of Basics and Applied Sciences Research (JOBASR) ISSN (print): 3026-9091, ISSN (online): 1597-9962

Volume 3(5) September 2025





Heat and Mass Transfer on Steady Incompressible Flow over a Continuously Moving Vertical Isothermal Surface with Uniform Suction and Chemical Reaction in the Presence of Soret–Dufour Effects



Yusuf Ya'u Gambo^{1*}, Mustapha Balogun², Bashir Yau Haruna³ & Auwalu Alhassan Girema ⁴ 1,2,3&4 Mathematics Department, Northwest University, Kano, Nigeria

*Corresponding Author Email: yygambo@gmail.com

ABSTRACT

Understanding coupled heat and mass transfer in viscous flows is essential for both industrial and biomedical applications, particularly where thermal gradients and concentration differences interact. This study addresses that gap by analysing the steady incompressible flow of a viscous fluid over a continuously moving isothermal vertical surface in the presence of Soret and Dufour effects with uniform suction. The nonlinear partial differential equations were reduced into ordinary differential equations with a specified boundary condition. The system of the governing partial differential equations was decoupled using the perturbation technique and the governing equations were solved analytically. Expressions for velocity, temperature, concentration were obtained and the effects of the main parameters were described. The velocity, temperature and concentration profiles as well as wall shear stress, Nusselt number and Sherwood number were presented graphically for realistic values of suction velocity (λ) , Prandtl number (P_r) , Schmidt number (s_c) as well as for arbitrary values of other parameters. It was observed that an increase in the Soret number (S_r) reduces the temperature but increases the velocity and concentration. Increasing Dufour parameter (D_f) raises both temperature and velocity, while reducing concentration. Notably, the Dufour effect exerted a stronger influence on thermal transport compared to mass diffusion. These results provide new insights into coupled heat and mass transfer in viscous flows over moving surfaces, with applications in industrial and biomedical systems.

Keywords:

Soret-Dufour effect; Isothermal surface; Suction; Heat and mass transfers

INTRODUCTION

The temperature gradient near a plate induces mass diffusion, which modifies the concentration profile within the boundary layer. Conversely, the Dufour (diffusion—thermo) effect generates an additional energy flux driven by concentration gradients, thereby altering the temperature distribution. When heat and mass transfer occur simultaneously in a moving fluid, the relations between fluxes and driving potentials become more complex than those described by Fourier's or Fick's laws alone. For example, Lagra *et al.* (2018) showed that an energy flux may be generated by composition gradients as well as by temperature gradients.

Early studies include Vajravelu and Sastri (1977), who obtained an exact solution for hydrodynamic boundary-layer flow and heat transfer over a continuously moving horizontal flat surface with uniform suction and internal heat generation/absorption.

Later, Vajravelu (1988) extended this problem to the vertical surface, analyzing both heating and cooling effects. The diffusion-thermo (Dufour) effect and thermo-diffusion (Soret) effect are reciprocal phenomena: Dufour refers to heat flux produced by concentration gradients, while Soret denotes mass flux driven by temperature gradients. In many studies, these cross-diffusion effects are neglected under assumption that their magnitudes are small compared to Fourier and Fick contributions. However, when species with different densities are introduced at a surface, or when significant concentration gradients exist, both Soret and Dufour effects can become important Jha and Ajibade (2010), Platten (2006).

Recent studies revisited these processes in various configurations. Jha and Gambo (2019) examined Soret and Dufour effects in unsteady free-convection mass transfer past a vertical plate.

Similarly, Mishra et al. (2023) and Sharma et al. (2012) analyzed Soret and Dufour effects in steady MHD mixed convection with thermal radiation and chemical reactions. More recently, influence of thermal diffusion on heat and mass transfer flow over a vertical channel with magnetic field intensity explored by Ibrahim et al. 2024 influence that increasing thermal Radiation leads to decrease the fluid temperature. Hamza et al. 2024 analysis investigated magnetized chemical reactions under Arrhenius control with Navier slip and convective boundary conditions. Their analysis revealed that fluid flow is enhanced by increasing the Navier slip parameter. In addition, Yau et al. (2025) reported a significant influence of the Dufour and thermal radiation on MHD blood flow through bifurcated arteries with heat source and chemical reaction, showing a reduction in biofluid under certain conditions.

Suction also modifies thermal and concentration profiles, influencing how Soret and Dufour manifest along the channel. Depending on the flow and thermal conditions, suction may enhance or suppress these effects by altering boundary-layer thickness and transfer rates Yasar (2007). The importance of suction/injection on steady fully developed mixed convection flow in a vertical parallel plate microchannel highlighted in the work of Jha and Aina (2018), who emphasized that the suction/injection may reach a considerable magnitude and cannot always be neglected.

To the best of our knowledge, a theoretical solution for hydrodynamic boundary-layer flow over a continuously moving isothermal vertical surface with uniform suction that simultaneously accounts for Soret and Dufour effects has not been fully developed. The present study addresses this gap by analyzing heat and mass transfer on a continuously moving vertical surface in the presence of Soret and Dufour effects, with suction velocity.

MATERIALS AND METHODS

We consider the steady, incompressible flow of a viscous fluid over a continuously moving isothermal vertical surface with uniform suction. The coordinate system is defined such that the x-axis lies along the surface in the upward direction of motion and the y-axis is normal to the surface. The velocity components in the x and y directions are u and v, respectively. Examples of such continuously moving surfaces include a metal plate extruded from a die or a filament drawn between feed and take-up rollers.

A small, constant suction velocity is imposed at the wall, removing fluid near the plate and thereby altering the boundary-layer structure, which in turn affects both velocity and thermal distributions. The flow is governed by the continuity, momentum, energy, and species-

conservation equations, with cross-diffusion effects (Soret and Dufour) explicitly included in the energy and mass equations. Appropriate boundary conditions are imposed at the surface (prescribed wall velocity, suction, wall temperature and concentration) and at infinity (ambient values and vanishing shear). The study provides the basis for examining the coupled heat and mass transfer effects in the presence of Soret and Dufour terms.

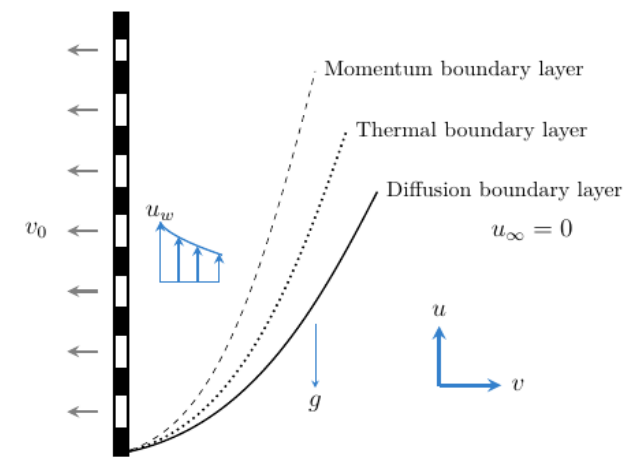


Figure (1): Geometry of the problem

Under the stated assumptions, the governing twodimensional boundary layer equations with Soret and Dufour effects are given by the Navier–Stokes, energy and concentration equations:

$$\frac{\partial u}{\partial x} + \frac{\partial u}{\partial y} = 0 \implies v_0 = \lambda,\tag{1}$$

$$\left(u\frac{\partial u}{\partial x} + v\frac{\partial u}{\partial y}\right) = \tau \frac{\partial^2 u}{\partial y^2} + g\beta(T - T_{\infty}) + g\beta'(C - C_{\infty}),$$
(2)

$$\rho C_{\rho} \left(u \frac{\partial T}{\partial x} + v \frac{\partial T}{\partial y} \right) = k \frac{\partial^{2} T}{\partial y^{2}} + D^{*} \frac{\partial^{2} C}{\partial y^{2}}, \tag{3}$$

$$u\frac{\partial C}{\partial x} + v\frac{\partial C}{\partial y} = D\frac{\partial^2 C}{\partial y^2} - k_1(C - C_{\infty}) + S^* \frac{\partial^2 T}{\partial y^2}, \quad (4)$$

The corresponding boundary conditions of equations are $u=u_w$, $T=T_w$, $C=C_w$ at y=0 $u=u_\infty$, $T\to T_\infty$, $C\to C_\infty$ as $y\to\infty$ (5)

SOLUTIONS TO THE PROBLEM

The governing equations with their corresponding boundary conditions are dimensional. They can be made dimensionless if the dependent and independent variables are redefined to be dimensionless by dividing them with constant reference properties appropriate to the flow. Therefore, by introducing the following variables, the following nondimensional quantities are introduced

$$Y = \frac{yv_0}{\eta}, U = \frac{u}{u_w}, G_r = \frac{\eta g \beta (T'_w - T'_{\infty})}{u_w v_0^2}, G_c = \frac{\eta g \beta^* (C'_w - TC'_{\infty})}{u_w v_0^2},$$

$$T = \frac{T' - T'_{\infty}}{T'_w - T'_{\infty}},$$

$$S_r = \frac{\eta}{T}, C = \frac{C' - C'_{\infty}}{T'_w - T'_{\infty}}, P_c = \frac{\eta C_p}{T'_w - T'_{\infty}}, D_c = \frac{D^* (T' - T'_{\infty})}{T'_w - T'_{\infty}}$$

$$S_{c} = \frac{\eta}{D}, \ C = \frac{C' - C'_{\infty}}{C'_{w} - C'_{\infty}}, \ P_{r} = \frac{\eta C_{p}}{k}, \ D_{f} = \frac{D^{*}(T' - T'_{\infty})}{k(T'_{w} - T'_{\infty})},$$

$$S_{t} = \frac{S^{*}(C' - C'_{\infty})}{D(C'_{w} - C'_{\infty})}, k_{r} = \frac{k_{1}\nu}{\nu_{0}^{2}}.$$

Here, P_r is the Prandtl number, S_c is the Schmidt number, G_r is the Grashof number, G_c is the modified Grashof number, S_t is the dimensionless Soret parameter and D_f is the dimensionless Dufour parameter, η kinematics viscosity, λ is the suction and k_r is the chemical reaction.

$$\frac{d^2U}{dY^2} + \lambda \frac{dU}{dY} + G_r T + G_c C = 0, \tag{6}$$

$$\frac{d^2T}{dY^2} + \lambda P_r \frac{dT}{dY} + D_f \frac{d^2C}{dY^2} = 0, \tag{7}$$

$$\frac{d^2C}{dY^2} + \lambda S_c \frac{dC}{dY} - S_c k_r C + S_t \frac{d^2T}{dY^2} = 0, \tag{8}$$

with boundary conditions
$$U = 1, \quad U = 1, \quad U = 1 \quad at \quad Y = 0 \\ U \to 0, \quad U \to 0, \quad U \to 0 \quad as \quad Y \to \infty$$
(9)

To derive analytical solutions to the coupled system of equations perturbation method is applied to decouple the equations using a small, nonzero parameter ϵ such that the Soret and Dufour parameters are of order $O\epsilon$. Utilizing the perturbation method to decouple the system of the governing equations, a very small parameter is introduced

$$T = T_0 + \epsilon T_1 + \cdots \tag{10}$$

$$C = C_0 + \epsilon C_1 + \cdots \tag{11}$$

$$U = U_0 + \epsilon U_1 + \cdots \tag{12}$$

Let

$$D_f = \epsilon b$$
 and $S_t = \epsilon a$,

where a and b are arbitrary constants of order O. Following perturbing the system of the governing equations, two cases can be obtained as follows:

Case I: Solutions for the zeroth order of ϵ

In this case, it can be observed that the temperature and concentration equations are independent of Soret and Dufour parameters, using equations (10)–(12) in the system of equations gives

$$\frac{d^2 U_0}{dY^2} + \lambda \frac{dU_0}{dY} + G_r T_0 + G_c C_0 = 0,$$
 (13)

$$\frac{d^2T_0}{dY^2} + \lambda P_r \frac{dT_0}{dY} = 0, (14)$$

$$\frac{d^2C_0}{dY^2} + \lambda S_c \frac{dC_0}{dY} - S_c k_r C_0 = 0,$$
 (15)

with the corresponding boundary conditions
$$U_0=1$$
, $T_0=1$, $C_0=1$ at $Y=0$ (16 $U_0\to 0$, $T_0\to 0$, $C_0\to 0$ as $Y\to \infty$

The following are the solutions of zeroth order of the parameter ϵ :

$$T_0 = e^{-\lambda P_r Y},\tag{17}$$

$$C_0 = e^{-\lambda_1 Y}. (18)$$

$$U_{0} = \left[1 + \frac{G_{r}}{\lambda P_{r}(\lambda P_{r} - \lambda)} + \frac{G_{c}}{\lambda_{1}(\lambda_{1} - \lambda)}\right] e^{-\lambda Y}$$

$$- \frac{G_{r}}{\lambda P_{r}(\lambda P_{r} - \lambda)} e^{-\lambda P_{r}Y}$$

$$- \frac{G_{c}}{\lambda_{1}(\lambda_{1} - \lambda)} e^{-\lambda_{1}Y}.$$
(19)

Case II: Solutions for the first order of ϵ In this case, the coupling of temperature and concentration equations are in terms of T_0 and C_0 which can be obtained as

$$\frac{d^2 U_1}{dY^2} + \lambda \frac{dU_1}{dY} + G_r T_1 + G_c C_1 = 0, \tag{20}$$

$$\frac{d^2T_1}{dY^2} + \lambda P_r \frac{dT_1}{dY} = -b \frac{d^2C_0}{dY^2},$$
 (21)

$$\frac{d^2C_1}{dY^2} + \lambda S_c \frac{dC_1}{dY} - S_c k_r C_1 = -a \frac{d^2 T_0}{dY^2}.$$
 (22)

with the corresponding boundary conditions
$$U_1=1$$
, $T_1=1$, $C_1=1$ at $Y=0$ (23 $U_1 \rightarrow 0$, $T_1 \rightarrow 0$, $C_1 \rightarrow 0$ as $Y \rightarrow \infty$.)

First order solutions to the temperature, concentration and velocity are

$$T_{1} = \left[1 + \frac{b\lambda_{1}^{2}}{\lambda_{1}(\lambda_{1} - \lambda P_{r})}\right]e^{-\lambda P_{r}Y} - \frac{b\lambda_{1}^{2}}{\lambda_{1}(\lambda_{1} - \lambda P_{r})}e^{-\lambda_{1}Y},$$
(24)

$$C_{1} = \left[1 + \frac{a(\lambda P_{r})^{2}}{\lambda P_{r}(\lambda P_{r} - \lambda Sc) - k_{r}S_{c}}\right]e^{-\lambda_{1}Y} - \frac{a(\lambda P_{r})^{2}}{\lambda P_{r}(\lambda P_{r} - \lambda Sc) - k_{r}S_{c}}e^{-\lambda P_{r}Y},$$
(25)

$$U_{1} = \begin{cases} 1 + G_{r} \left[\frac{1}{\lambda_{1}(\lambda_{1} - \lambda)} \left(1 + \frac{b\lambda_{1}^{2}}{\lambda_{1}(\lambda_{1} - \lambda P_{r})} \right) \right] \\ -b\lambda_{1}^{2} \\ -G_{m} \left[\frac{1}{\lambda_{1}(\lambda_{1} - \lambda)} \left(1 + \frac{a(\lambda P_{r})^{2}}{\lambda P_{r}(\lambda P_{r} - \lambda Sc) - k_{r}S_{c}} \right) \right] \\ -a(\lambda P_{r})^{2} \\ -\frac{a(\lambda P_{r})^{2}}{[\lambda P_{r}(\lambda P_{r} - \lambda)][\lambda P_{r}(\lambda P_{r} - \lambda Sc) - k_{r}S_{c}]} \end{cases} \end{cases}$$

$$-G_{r} \begin{bmatrix} \frac{1}{\lambda_{1}(\lambda_{1} - \lambda)} \left(1 + \frac{b\lambda_{1}^{2}}{\lambda_{1}(\lambda_{1} - \lambda P_{r})} \right) e^{-\lambda_{1}Y} \\ -\frac{b\lambda_{1}^{2}e^{-\lambda P_{r}Y}}{[\lambda P_{r}(\lambda P_{r} - \lambda)][\lambda_{1}(\lambda_{1} - \lambda P_{r})]} \end{bmatrix}$$

$$-G_{c} \begin{bmatrix} \frac{1}{\lambda_{1}(\lambda_{1} - \lambda)} \left(1 + \frac{a(\lambda P_{r})^{2}}{\lambda P_{r}(\lambda P_{r} - \lambda Sc) - k_{r}S_{c}} \right) e^{-\lambda_{1}Y} \\ -\frac{a(\lambda P_{r})^{2}e^{-\lambda P_{r}Y}}{[\lambda P_{r}(\lambda P_{r} - \lambda)][\lambda_{1}(\lambda_{1} - \lambda P_{r})]} \end{bmatrix}$$

$$(26)$$

Therefore, by combining the case I and case II solutions, the final analytical solutions for temperature, concentration and velocity are respectively presented below

$$T(Y) = e^{-\lambda P_r Y} + \left[\epsilon + \frac{D_f \lambda_1^2}{\lambda_1 (\lambda_1 - \lambda P_r)}\right] e^{-\lambda P_r Y} - \frac{D_f \lambda_1^2}{\lambda_1 (\lambda_1 - \lambda P_r)} e^{-\lambda_1 Y},$$
(27)

$$C(Y) = e^{-\lambda_1 Y} + \left[\epsilon + \frac{S_t(\lambda P_r)^2}{\lambda P_r(\lambda P_r - \lambda Sc) - k_r S_c}\right] e^{-\lambda_1 Y}$$

$$-\frac{S_t(\lambda P_r)^2}{\lambda P_r(\lambda P_r - \lambda Sc) - k_r S_c} e^{-\lambda P_r Y},$$
(28)

$$U(Y) = \begin{cases} 1 + \epsilon + \frac{G_r}{\lambda_1(\lambda_1 - \lambda)} \left[1 + \left(\epsilon + \frac{S_t \lambda_1^2}{\lambda_1(\lambda_1 - \lambda P_r)} \right) \right] \\ - \frac{G_r S_t \lambda_1^2}{[\lambda P_r (\lambda P_r - \lambda)] [\lambda_1(\lambda_1 - \lambda P_r)]} \\ - \frac{G_c}{\lambda_1(\lambda_1 - \lambda)} \left[1 - \left(\epsilon + \frac{D_f (\lambda P_r)^2}{\lambda P_r (\lambda P_r - \lambda Sc) - k_r S_c} \right) \right] \\ - \frac{D_f (\lambda P_r)^2}{[\lambda P_r (\lambda P_r - \lambda)] [\lambda P_r (\lambda P_r - \lambda Sc) - k_r S_c]} \end{cases}$$

$$+ \left[\frac{G_r S_t \lambda_1^2}{[\lambda P_r (\lambda P_r - \lambda)] [\lambda_1(\lambda_1 - \lambda P_r)]} - \frac{G_r}{\lambda P_r (\lambda P_r - \lambda)} \right] e^{-\lambda P_r Y}$$

$$- \frac{G_c}{\lambda_1(\lambda_1 - \lambda)} \left[1 - \left(\epsilon + \frac{D_f (\lambda P_r)^2}{\lambda P_r (\lambda P_r - \lambda Sc) - k_r S_c} \right) \right] e^{-\lambda_1 Y}$$

$$- \frac{G_r}{\lambda_1(\lambda_1 - \lambda)} \left(\epsilon + \frac{S_t \lambda_1^2}{\lambda_1(\lambda_1 - \lambda P_r)} \right) e^{-\lambda_1 Y}$$

$$+ \left[\frac{G_c D_f (\lambda P_r)^2}{[\lambda P_r (\lambda P_r - \lambda)] [\lambda_1(\lambda_1 - \lambda P_r)]} \right] e^{-\lambda P_r Y}$$

$$Sh = -\frac{dC}{dY}\Big|_{Y=0},\tag{32}$$

WALL SHEAR STRESS, NUSSELT NUMBER AND SHERWOOD NUMBER

The wall shear stress, heat and mass transfer coefficients are the physical quantities considered in this study. Nusselt number (Nu) is defined by

$$Nu = -\frac{dT}{dY}\Big|_{Y=0},\tag{30}$$

$$Sh = (1 + \epsilon)\lambda_1 + (\lambda_1 - \lambda P_r) \frac{S_t(\lambda P_r)^2}{\lambda P_r(\lambda P_r - \lambda Sc) - k_r S_c}.$$
(33)

The expressions for the wall shear stress (WSS) is defined as

$$Nu = (1 + \epsilon)\lambda P_r + (1 + \lambda_1) \frac{D_f \lambda_1}{(\lambda_1 - \lambda P_r)}.$$
 (31)
$$WSS = -\eta \frac{dU}{dY} \Big|_{Y=0},$$
 (34)

Sherwood number (Sh) is expressed as

$$WSS = \mu \begin{bmatrix} 1 + \epsilon + \frac{G_r}{\lambda_1(\lambda_1 - \lambda)} \left[1 + \left(\epsilon + \frac{S_t \lambda_1^2}{\lambda_1(\lambda_1 - \lambda P_r)} \right) \right] \\ - \frac{G_r S_t \lambda_1^2}{[\lambda P_r (\lambda P_r - \lambda)] [\lambda_1(\lambda_1 - \lambda P_r)]} \\ - \frac{G_c}{\lambda_1(\lambda_1 - \lambda)} \left[1 - \left(\epsilon + \frac{D_f (\lambda P_r)^2}{\lambda P_r (\lambda P_r - \lambda Sc) - k_r S_c} \right) \right] \\ - \frac{D_f (\lambda P_r)^2}{[\lambda P_r (\lambda P_r - \lambda)] [\lambda P_r (\lambda P_r - \lambda Sc) - k_r S_c]} \end{bmatrix}$$

$$+ \lambda P_r \left[\frac{G_r S_t \lambda_1^2}{[\lambda P_r (\lambda P_r - \lambda)] [\lambda_1(\lambda_1 - \lambda P_r)]} - \frac{G_r}{\lambda P_r (\lambda P_r - \lambda)} \right] \\ + \lambda P_r \frac{G_c D_f (\lambda P_r)^2}{[\lambda P_r (\lambda P_r - \lambda)] [\lambda_1(\lambda_1 - \lambda P_r)]} \\ - \frac{G_r}{\lambda_1(\lambda_1 - \lambda)} \left[-\frac{G_r}{\lambda_1(\lambda_1 - \lambda)} \left[1 - \left(\epsilon + \frac{D_f (\lambda P_r)^2}{\lambda P_r (\lambda P_r - \lambda Sc) - k_r S_c} \right) \right] \right]$$

RESULTS AND DISCUSSION

Authors have investigated the effects of Soret and Dufour parameters on heat and mass transfer in a steady incompressible flow of a viscous fluid over a continuously moving isothermal vertical surface with uniform suction. The analytical solutions to the system of the governing equations with appropriate initial and boundary conditions have been obtained using perturbation method. The results are obtained by varying the values of the embedded parameters. The Soret parameter (S_t) , Dufour parameter (D_f) , suction (λ) , Grashof number (G_r) and modified Grashof number (G_c) are arbitrarily taken. During the course of analytical computations of the velocity, temperature, concentration, coefficient of wall shear stress, heat and mass transfer coefficients, the values of Prandtl number (P_r) are nominated for mercury $(P_r = 0.025)$, air $(P_r = 0.7)$ at 20°C, pure water ($P_r = 7.0$). S_c Similarly, the values of the Schmidt number (S_c) are chosen for the gases representing diffusing chemical species of most common interest in air, namely hydrogen ($S_c = 0.22$), water-vapour ($S_c = 0.60$), ammonia ($S_c = 0.78$), methanol and propyl benzene (S_c = 2.62) at 20°C and one atmospheric pressure. The solutions for temperature, concentration, velocity, coefficient of heat transfer, coefficient of mass transfer and skin friction are graphically reported in Figures thereby revealing the influence of the embedded parameters on the flow. It is important to state that when Soret and Dufour effects are absent, that is when $S_t =$ $D_f = 0$, the results in equations correspond exactly to the work in Muthucumaraswamy (2002). The identified parameters are set default at $\lambda = 1, P_r = 0.71, S_c =$ $0.6, k_r = 0.2, D_f = S_t = 0.3, G_r = 2, G_c = 1.5, \ \mu = 1.$

The solutions for the governing equations are graphically reported in Figures 2-18. Figures 2-5 present the influences of Soret and Dufour effects on the temperature, concentration and velocity profiles. In Figure 2, it can be seen that the variation of the velocity boundary layer with the Dufour effect (D_f) . It is notably observed that the fluid velocity boundary layer thickness decreases with an increase in the Dufour effect. Figure 3 shows the variation of the thermal boundary-layer with the Dufour effect. It is noticed that the thermal boundary layer thickness increases with an increase in the Dufour effect. The concentration reduces rapidly and diffuses more gradually when the thermal diffusivity is dominated.

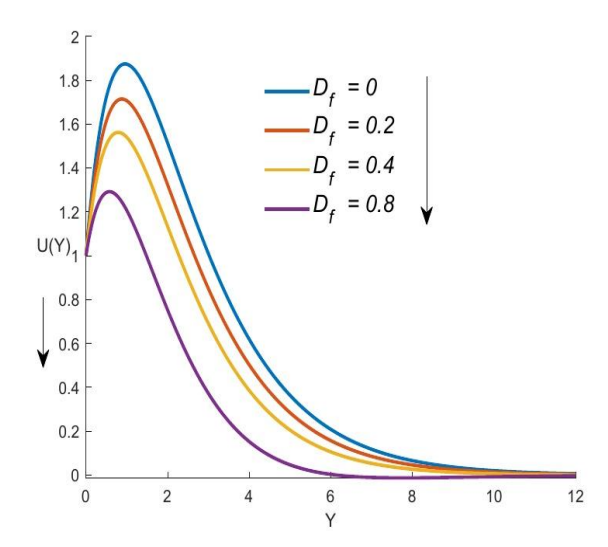


Figure 2: Velocity profile for different values of D_f .

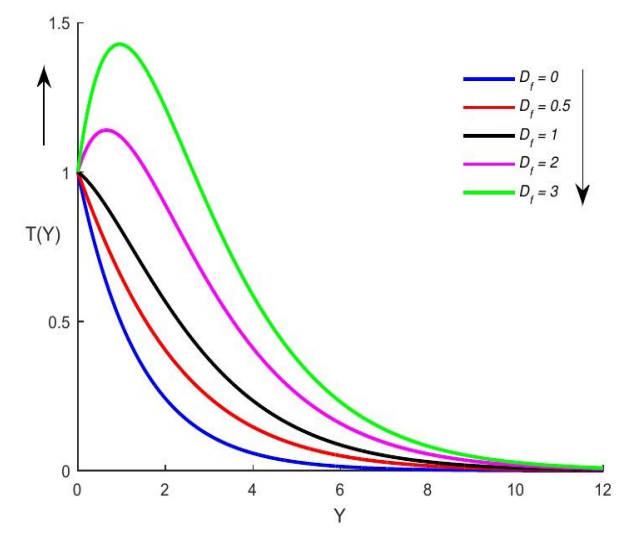


Figure 3: Temperature profile for different values of D_f . In Figures 4 and 5, the influence of Soret effect (S_t) on temperature and concentration profiles in a fluid flow is illustrated. The Soret effect (S_t) refers to temperature gradient driving concentration gradient. In Figure 4, it can be seen that when Soret effect increases, the fluid velocity decreases notably owing to the effect of strong crossdiffusion where concentration gradient generates additional heat flux. Moreover, the enhancement in Soret effect suppress buoyancy-driven motion which results reduction in the peak velocity and thinner momentum boundary layers. In Figure 5, It is seen that the thermal diffusion significantly affects mass transfer. Since the surface is isothermal, it maintains a steady thermal gradient that strengthens the Soret effect. The uniform suction stabilizes the boundary layer, allowing clear observation of how S_t affects concentration. For $S_t = 0$, the concentration starts reducing and diffuses more gradually. Moreover, the mass concentration at the wall

increases and the peak concentration shifts higher with an increase in S_t .

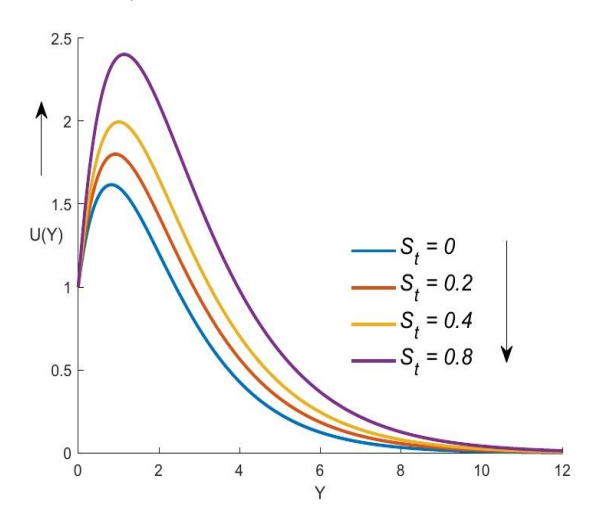


Figure 4: Velocity profile for different values of S_t .

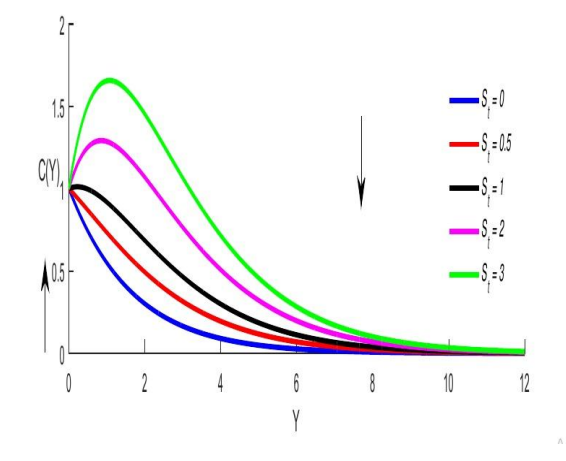


Figure 5: Concentration profile for different values of S_t . The significant effect of Schmidt number on velocity, temperature and con centration profiles are depicted in Figure 6-8. Figure 6 illustrates the influence of Schmidt number on the velocity profile. The analysis reveals that when Schmidt number (S_c) increases, the rise of the velocity profile becomes more pronounced, while the boundary layer thickness de creases. This behaviour is attributed to the reduction in mass diffusivity associated with higher Schmidt number (S_c) , which limits the spread of momentum (or mass) away from the surface. Figure 7 displays the temperature distribution with varying values of Schmidt number. It is seen that an increase in Schmidt number there is a rise in maximum temperature near the wall. It is noticed that the transition about Y = 2 is due to a shift in dominance from convective to diffusive transport mechanisms. For different values of Schmidt number, the transition region where molecular diffusion dominates over convective transport shifts is due to the

variations. From this Figure 8, the outcomes indicate that the enhancement in Schmidt number (S_c) leads to decrease in concentration. This causes the influence of concentration buoyancy to diminish as result in a decline in the concentration. The depletion of the concentration is accompanied by instantaneous depletion in the concentration boundary layers, which is perceptible from the surface.

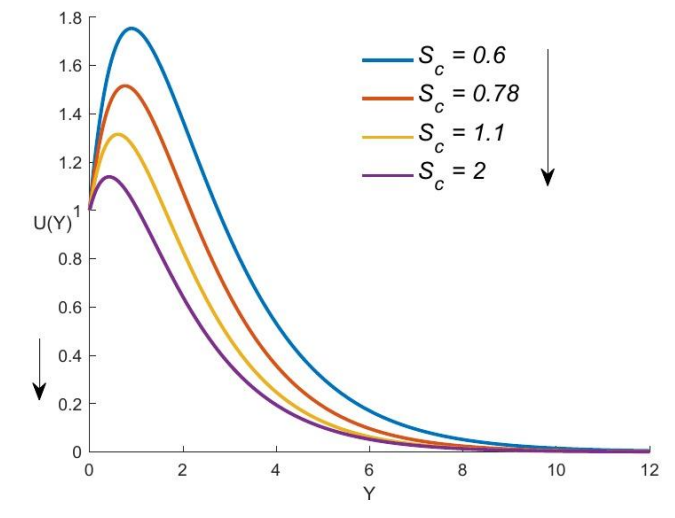


Figure 6: Velocity profile for different values of S_c .

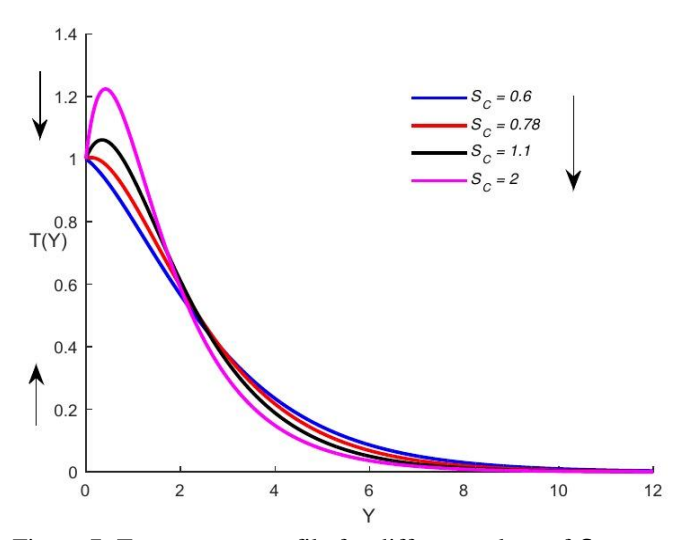


Figure 7: Temperature profile for different values of S_c .

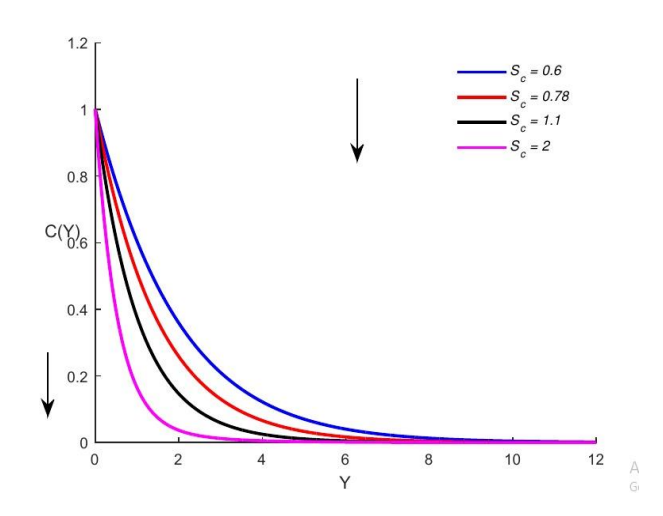


Figure 8: Concentration profile for different values of S_c .

Figure 9 demonstrates the effect of varying Prandtl number (P_r) on the velocity profile. The results show that the peak velocity within the boundary layer reduces with an increase in Prandtl number. This indicates slower thermal diffusion relative to momentum diffusion, thereby reducing buoyancy-induced flow. behaviour is significant in thermal-fluid systems, where selecting appropriate working fluids with tailored Prandtl number. In Figure 10, it is illustrated that the enhancement in Prandtl number (P_r) , there is a decrease in temperature. This causes the influence of temperature buoyancy to diminish as result in a decline in the temperature. Figure 11 depicts the impact of the Prandtl number (P_r) on the concentration profile with varying P_r . It is seen that an increase in Prandtl number leads to a rise in peak concentration near the wall. This shows that heat conduction (thermal diffusion) significantly affects mass transport. The concentration boundary layer thickness decreases with in creasing P_r . Additionally, the concentration is more stretched out when diffusion dominates over convection with a decrease in Prandtl number (below 1). However, the heat is retained near the surface when the thermal diffusivity is lower with an increase in Prandtl number (above 1) which enhances temperature gradient and indirectly strengthens buoyancy effect and concentration gradient. Since suction (λ) is applied, it stabilizes the boundary layer, by reducing concentration fluctuations. It is seen that the occurrence at Y = 2 is due to a shift in dominance from convective to diffusive transport mechanisms. For different values of P_r , the transition region where molecular diffusion dominates over convective transport shifts is due to the variations.

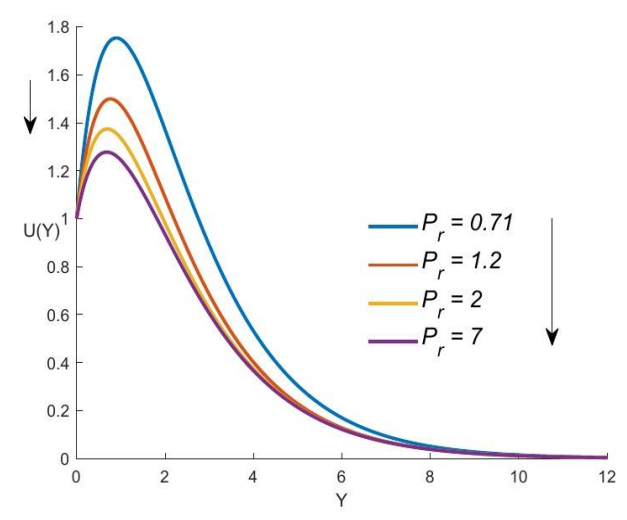


Figure 9: Velocity profile for different values of P_r .

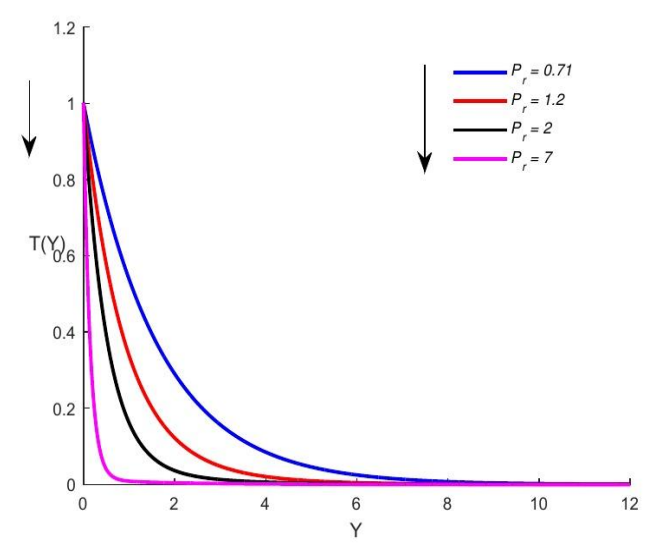


Figure 10: Temperature profile for different values of P_r .

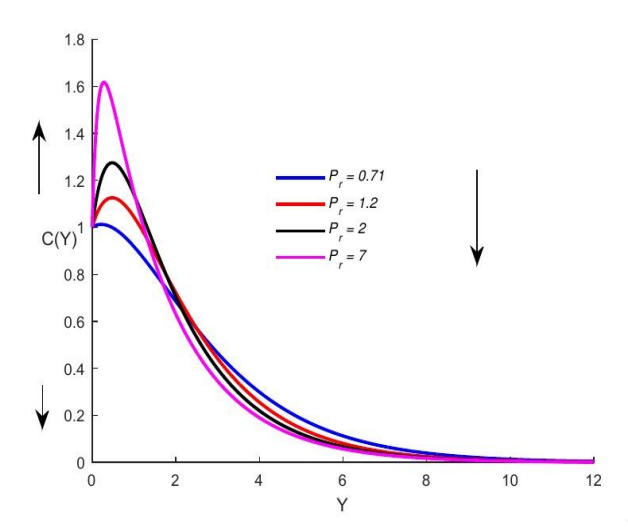


Figure 11: Concentration profile for different values of P_r .

The effect of suction parameter on velocity, temperature and concentration profiles in the boundary layer are depicted in Figure 12-14. The Figure 12 depicts that when suction (λ) increases with a decrease in the peak velocity profile which is slowly flattened and compressed such behaviour indicate a thinner momentum boundary layer due to dominant suction effect over buoyancy forces. In Figure 13 and 14, the temperature and concentration profiles start at 1 (non-dimensional surface temperature and concentration) and asymptotically approaches 0 as Y in creases i.e., moving away from the surface into the ambient fluid. It is indicated that the stronger suction pulls cooler fluid from outside closer to the wall, decreasing the fluid temperature and concentration near the surface more effectively. As suction (λ) increases, the thermal boundary layer becomes thinner. It is seen that for $\lambda = 0$ (no suction), velocity increases to a maximum peak while the temperature and concentration then gradually decays to zero as $Y \to \infty$.

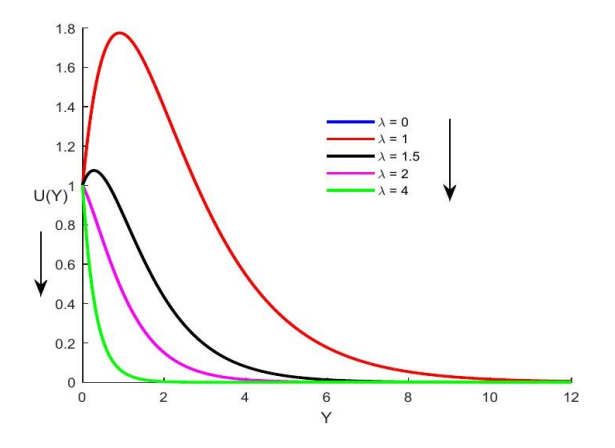


Figure 12: Velocity profile for different values of λ .

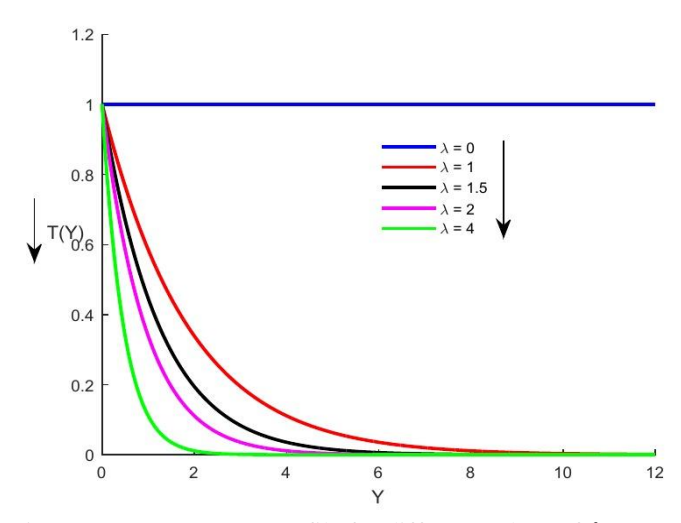


Figure 13: Temperature profile for different values of λ .

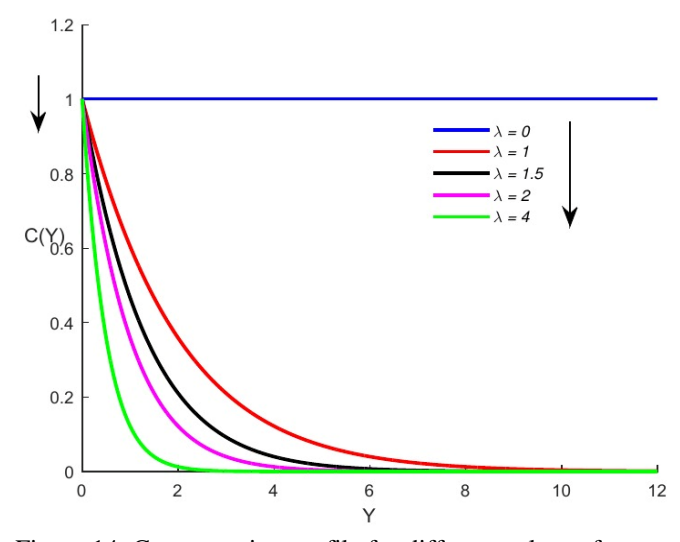


Figure 14: Concentration profile for different values of λ .

Figures 14-17 display the influence of chemical reaction on velocity, temperature and concentration profiles respectively. The velocity profile decreases progressively with increasing values of the chemical reaction parameter, highlighting the damping effect of chemical reactions on fluid motion as shown in Figure 14. Whereas, Figure 15 reveals that the temperature profile is comparatively insensitive to variations in the chemical reaction parameter, indicating that chemical reactions exert a relatively minor influence on thermal distribution. Furthermore, Figure 17 illustrates that the concentration profile diminishes with increasing chemical reaction rates, demonstrating that chemical reactions can substantially alter mass diffusion within the system.

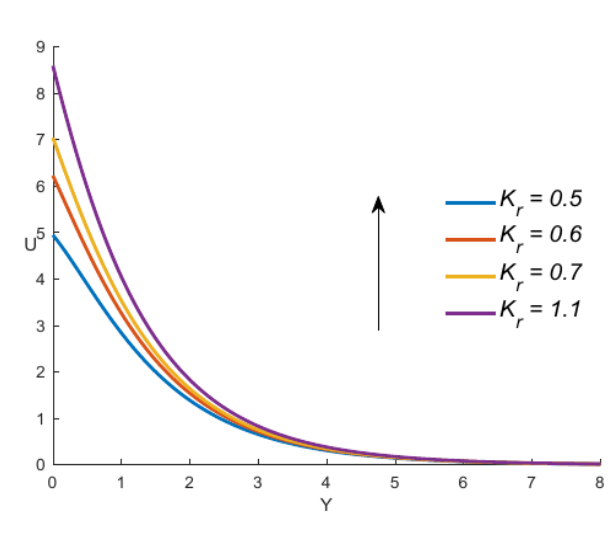


Figure 15: Velocity profile for different values of k_r .

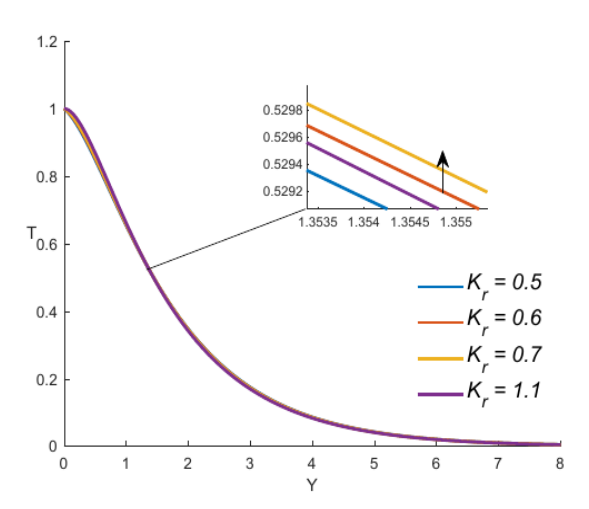


Figure 16: Temperature distribution for different values of k_r .

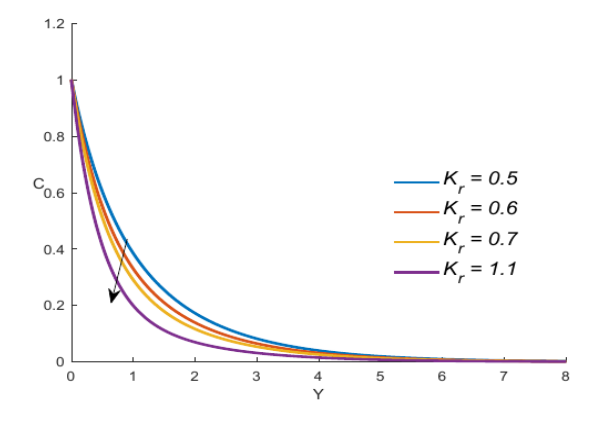


Figure 17: Concentration profile for different values of k_r .

Figure 18 illustrates the comparison between the velocity profile analysis conducted by Muthucumaraswamy (2002) and the current study. Figure 18a portrays the variation of k_r in the absent of Soret and Dufour Effects, indicating minimal growing in concentration while, Figure 18b depicts the variation of k_r in the presence of Soret and Dufour Effects. The declination in concentration when k_r is low gives a boost to thermal diffusion and diffusion—thermo and intensifies the thermal boundary layer so that fluid velocity increase with growing chemical reaction parameter.

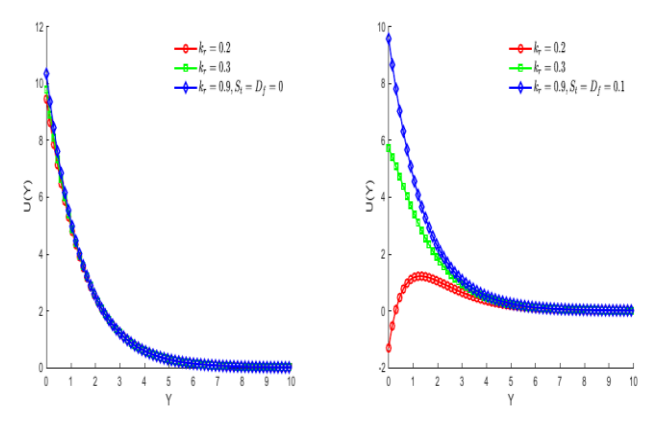


Figure 18: Comparison between the work of Muthucumaraswamy (2002) and the present work.

Table 4.1 illustrates the wall shear stress (WSS) at the surface for fluid velocity. From this table, the increase in G_r (Grashof number for heat transfer) and G_c (Grashof number for mass transfer) escalate WSS. This trend indicates that stronger thermal and solutal buoyancy effects promote convective motion, thereby intensifying near wall velocity gradients and increasing shear stress. But contrary repercussions were eventuated in case of λ , D_f and S_t . It is evident that an increase in suction λ leads to increase in WSS owing to the resistive force or viscous drag on the surface due to a thinner boundary layer.

Table 4.1: Variation of wall shear stress for different values of the embedded parameters at (Y = 0). The variations of the parameter values are indicated in bold.

| λ | G_r | G_c | P_r | Sc | D_f | S_t | $	au_w$ |
|-----------|----------|----------|------------|------|-------|------------|-------------|
| 2 | 1 | 1 | 0.7 | 0.60 | 0.1 | 0.1 | -0.19584524 |
| 1 | 2 | 1 | 0.7 | 0.60 | 0.1 | 0.1 | -2.53688095 |
| 1 | 4 | 1 | 0.7 | 0.60 | 0.1 | 0.1 | -3.82426190 |
| 1 | 1 | 2 | 0.7 | 0.60 | 0.1 | 0.1 | -3.64319048 |
| 1 | 1 | $\bf 4$ | 0.7 | 0.60 | 0.1 | 0.1 | -7.14319048 |
| 1 | 1 | 1 | 7.0 | 0.60 | 0.1 | 0.1 | -1.31461905 |
| 1 | 1 | 1 | ${\bf 21}$ | 0.60 | 0.1 | 0.1 | -1.27176190 |
| 1 | 1 | 1 | 0.7 | 0.22 | 0.1 | 0.1 | -4.91735714 |
| 1 | 1 | 1 | 0.7 | 0.78 | 0.1 | 0.1 | -1.48915201 |
| 1 | 1 | 1 | 0.7 | 0.60 | 0.5 | 0.1 | -1.60747619 |
| 1 | 1 | 1 | 0.7 | 0.60 | 0.0 | 0.1 | -1.96461905 |
| 1 | 1 | 1 | 0.7 | 0.60 | 0.1 | 0.5 | -2.22652381 |
| 1 | 1 | 1 | 0.7 | 0.60 | 0.1 | 0.0 | -1.80985714 |

Variations in the Soret and Dufour numbers significantly influence WSS. It is clear that WSS decreases as the Dufour number increases. This indicates that the stronger heat transfer impacts on velocity gradients. While, the WSS decreases with increase in Soret number which shows that temperature-driven mass diffusion weakens near wall shear stress.

From Table 4.2: The augmentation in suction λ results in exponential amplification of both Nu and Sh, signifying a profound intensification of convective transport

phenomena. The imposition of suction attenuates boundary layer thickness, thereby enhances the interfacial exchange rates for both thermal energy and mass species. An increment in P_r precipitates a surge in Nu. This arises due to the inverse correlation between P_r and thermal diffusivity, wherein a larger P_r culminates in more constricted thermal boundary layers, thereby escalates the temperature gradient near the surface and amplifies convective heat dissipation.

Table 4.2: Variation of heat and mass transfer coefficients for different embedded values parameters. The variations of the parameter values are indicated in bold.

| λ | P_r | Sc | S_t | D_f | Sh | Nu |
|---|------------|------|-------|-------|---------|--------|
| 2 | 0.7 | 0.6 | 0.1 | 0.1 | 1.0612 | 1.2814 |
| 1 | 7.0 | 0.6 | 0.1 | 0.1 | -0.0994 | 6.9470 |
| 1 | ${\bf 21}$ | 0.6 | 0.1 | 0.1 | -1.4994 | 20.961 |
| 1 | 0.7 | 0.22 | 0.1 | 0.1 | 0.15022 | 0.6787 |
| 1 | 0.7 | 0.78 | 0.1 | 0.1 | 0.71078 | 0.6227 |
| 1 | 0.7 | 0.6 | 0.5 | 0.1 | 0.25060 | 0.6407 |
| 1 | 0.7 | 0.6 | 0.0 | 0.1 | 0.60060 | 0.6407 |
| 1 | 0.7 | 0.6 | 0.1 | 0.5 | 0.53060 | 0.4007 |
| 1 | 0.7 | 0.6 | 0.1 | 0.0 | 0.53060 | 0.7007 |

It is perceived that the higher Schmidt numbers impede mass diffusivity, resulting in an intensified concentration gradient that fosters superior mass transfer. A pronounced increase in S_c engenders a substantial elevation in Sh. A discernible depreciation in Nu is observed as D_f increases, implying that heat diffusion.

CONCLUSION

This study provides complete analytical solutions for the uniform suction in a continuously moving isothermal vertical surface on heat and mass transfer flow in the presence of Soret and Dufour effects for different situations. Finding analytical solutions for such mathematical model's time independent flows is less difficult due to coupling of heat and mass transfer. This work is the generalization of the mathematical model of Muthucumaraswamy (2002). Based on this research, noteworthy results are summarized as follows:

- The velocity decreases with an increase in Dufour number, Schmidt number, suction velocity and Prandtl number. On the other hand, the Soret number enhances the velocity, underscoring the role of mass diffusion induced by thermal gradients.
- The temperature distribution decreases with increasing Prandtl number, Schmidt number and suction velocity indicating enhanced thermal diffusion and convective cooling. Conversely,

an increase in the Dufour number elevates the temperature field, emphasizing the strong coupling between mass diffusion and thermal energy.

- The concentration profile increases with an increase in Soret number whereas it is diminished by larger Schmidt number, suction velocity, and Prandtl number. This demonstrates the competitive balance between thermally induced diffusion and mass diffusivity.
- Wall shear stress decreases with an increase in Soret number and Dufour number, while it rises with increases in suction velocity, Grashof number and modified Grashof number. It is indicated that the buoyancy and suction effects counteract the weakening of wall shear induced by coupled diffusion phenomena.
- The Sherwood number is increased with the increase in Schmidt number, Soret number and suction velocity, confirming the strong dependence of mass transfer on diffusivity and cross-diffusion effects.
- The normal velocity decreases with increasing decay parameter and tending to zero very fast for higher values of the decay parameter.

REFERENCE

Hamza, M.M., Isa, M.M., Ibrahim, Y. and Usman, H. (2024.). Analysis of magnetized chemical reaction under arrhenius control in the presence of navier slip and convective boundary conditions. Journal of Basics and Applied Sciences Research, 2(2):71–82. https://doi.org/10.33003/jobasr-2024-v2i2-54.

brahim, Y., Adamu, I., Ibrahim, U.T. and Sa'adu A. (2024.). Influence of thermal diffusion (soret term) on heat and mass transfer flow over a vertical channel with magnetic field in tensity. *Journal of Basics and Applied Sciences Research*, 2(2):60–70, ISSN 3026 9091, ISSN (online): 1597-9962. https://doi.org/10.33003/jobasr-2024-v2i253.

Jha, B. and Ajibade, A. O. (2010). Free convection heat and mass transfer flow in a vertical channel with the Dufour effect. *Proceedings of the Institution of Mechanical Engineers, Part E: Journal of Process Mechanical Engineering*, 224(2):91–101.

Jha, B. K. and Aina, B. (2018). Role of suction/injection on steady fully developed mixed convection flow in a vertical parallel plate microchannel. *Ain Shams Engineering Journal*, 9(4):747–755.

Jha, B. K., and Gambo, Y. (2019). Unsteady free convection and mass transfer flow past an impulsively started vertical plate with Soret and Dufour effects: an analytical approach. *SN Applied Sciences*. 1, article 1234. https://link.springer.com/article/10.1007/s42452-019-1246-1

Lagra, A., Bourich, M., Hasnaoui, M., Amahmid, A., and Er-Raki, M. (2018). Analytical and numerical study of Soret and Dufour effects on double diffusive convection in a shallow horizontal binary fluid layer sub mitted to uniform fluxes of heat and mass. *Mathematical Problems in Engineering*, 2018(1):7946078

Mishra, N. K. (2023). Computational analysis of Soret and Dufour effects on nanofluid flow through a stenosed artery in the presence of temperature dependent viscosity. *Acta Mechanica*, 7(2):246–253.

Muthucumaraswamy, R. (2002). Effects of a chemical reaction on a moving isothermal vertical surface with suction. *Acta Mechanica*, 155(1):65–70.

Sharma, B., Yadav, K., Mishra, N., and Chaudhary, R. (2012). Soret and Dufour effects on unsteady MHD

mixed convection flow past a radiative vertical porous plate embedded in a porous medium with chemical reaction. *Journal of Applied Mathematics*, *3*, 717–723. https://doi.org/10.4236/am.2012.37105.

Patten, J. K. (2006). The Soret effect: A review of recent experimental results. *Journal of Applied Mechanics*, 73(1), 5–15. https://doi.org/10.1115/1.1992517.

Vajravelu, K. (1986). Hydromagnetic flow and heat transfer over a continuous moving surface. *Acta Mechanica*, **64**: 197-185.

Vajravelu, K. (1988). Hydromagnetic convection at continuous moving surface. *Acta Mechanica*, **72**: 223-232.

Yasar, D (2007). Non-equilibrium thermodynamics. Transport and rate processes in physical, chemical and biological systems. *Elsevier*.

Yau, Y. G., Yau B. H., and Girema A. A. (2025). Impact of Dufour and Thermal Radiation on unsteady MHD Blood Flow through Bifurcated Arteries with Heat Source and Chemical Reaction: *Journal of Basics and Applied Sciences Research*, Volume-3, Issue-3. https://dx.doi.org/10.4314/jobasr.v3i3.32.

APPENDIX

NOMENCLATURE

- *e* Exponential function
- S_c Schmidt number
- P_r Prandtl number
- C_p Specific heat
- D Mass diffusion coefficient
- k Thermal conductivity
- g Acceleration due gravity
- *Nu* Nusselt number
- Sh Sherwood number
- T' Dimensional temperature
- T_w Wall temperature
- C' Dimensional concentration
- C_w Wall concentration
- *D** Dimensional Dufour parameter
- S* Dimensional Soret parameter
- *G_c* Mass Grashof number
- G_r Thermal Grashof number
- u_w Dimensional velocity of the vertical surface
- u, v Velocity components in the x, y-directions, respectively
- x Spatial coordinate along the surface
- y Spatial coordinate normal to the surface

WSS Wall shear stress

 k_1 Rate of chemical reaction

Heat and Mass Transfer on Steady ...

Yusuf et al.

JOBASR2025 3(5): 173-186

- K Chemical reaction
- C Dimensionless concentration
- T Dimensionless temperature
- U Dimensionless velocity
- Y Dimensionless spatial coordinate normal to the surface

Greek Symbols

- β Volumetric coefficient due to thermal expansion
- β^* Volumetric coefficient due to concentration expansion

- ρ Density of fluid
- τ Kinematic viscosity
- λ suction velocity
- η Kinematic viscosity

Subscripts

- w Conditions on the wall
- ∞ Free stream condition